Novel template synthesis and characterization of chitosan–silica composite: evaluation of sorption characteristics of cadmium(II) and lead(II) by mesoporous chitosan–silica composite

Lalchhingpuii[a], Diwakar Tiwari[a], Sang-Il Choi[b], Lalhmunsiama[c], Seung-Mok Lee[c],*

[a]*Department of Chemistry, School of Physical Sciences, Mizoram University, Aizawl 796004, India, Tel. +918014602102; email: achhingi.pc@gmail.com (Lalchhingpuii), Tel. +91-9862323015; email: diw_tiwari@yahoo.com (D. Tiwari)*
[b]*Department of Environmental Engineering, Kwangwoon University, Seoul 01897, Korea, Tel. +82-2-940-5183; email: sichoi@kw.ac.kr (S.-I. Choi)*
[c]*Department of Environmental Engineering, Catholic Kwandong University, 522 Naegok-dong, Gangneung 210-701, Korea, Tel. +82-33-649-7535; Fax: +82-33-642-7635; email: leesm@cku.ac.kr (S.-M. Lee), Tel. +82-10-5188-4535; email: lhsiama27@gmail.com (Lalhmunsiama)*

ABSTRACT

Template synthesis was carried out to obtain mesoporous chitosan–silica (M-CS) composite employing natural chitosan and trimethoxy(octyl)silane (TMOS) as precursor materials. Initially, TMOS was grafted with chitosan polymer to obtain a composite material and then annealed at 500°C to obtain the M-CS. The Brunauer, Emmett and Teller specific surface area and pore size of the M-CS solid were found to be 371.77 m^2/g and 3.62 nm, respectively. Energy dispersive X-ray spectroscopy analytical data confirmed the presence of silica and the X-ray diffraction analysis indicated the amorphous nature of the solid. Moreover, the Fourier-transform infrared analysis indicated the presence of Si–O–Si condensed phase network. The M-CS composite was intended to utilize in the remediation of aquatic environment contaminated with potential water pollutant cadmium(II) and lead(II) under the batch and column reactor operations. The concentration dependence data were fitted well to the Langmuir adsorption model and the Langmuir monolayer sorption capacities were found to be 5.208 and 4.587 mg/g, respectively, for the cadmium(II) and lead(II). M-CS composite was found efficient adsorbing material for the removal of cadmium(II) and lead(II) since an apparent equilibrium between solid/solution interface was achieved within 120 and 60 min, respectively. Moreover, the kinetic data are fitted well to the pseudo-second-order and fractal-like-pseudo-second-order kinetic models. The 1,000 times increase in background electrolyte concentrations (NaNO$_3$) did not affect significantly the percentage removal of cadmium(II) by the M-CS indicated that the toxic ions are forming an inner-sphere complexes with relatively stronger chemical forces onto the solid surface. A high breakthrough volume was obtained in the fixed bed column study and the breakthrough data were fitted well to the non-linear Thomas equation. The estimated loading capacity for cadmium(II) in a column packed with M-CS composite was found to be 11.65 mg/g.

Keywords: Mesoporous; Silica; Chitosan; Cd(II); Pb(II); Fixed-bed column

* Corresponding author.

1. Introduction

The ordered mesoporous silica possessed several useful properties viz., thick pore wall, interconnected large mesopores and high surface area with enhanced hydrothermal/thermal/mechanical stability, etc. [1]. This enabled porous silica to utilize for various applications in the field of pharmaceutical sciences [2–4], environmental remediation [5,6], photocatalytic advanced oxidation processes [7], sensors [8], corrosion resistance [9], etc. Additionally, these materials are shown useful applications in catalysis [10], bioseparation [11], medical contrasting [12], food technology [13], etc. The mesoporous silica is known to be an excellent carrier for drug delivery in biosystem because of its encapsulation of drug molecules within the nanopores or mesopores which enhances the release of poorly soluble drugs. Moreover, the nanopores present in silica framework suppress significantly the crystallization of drug molecules that restricts the growth of nanoparticles. Therefore, the dissolution velocity, saturation solubility and storage stability of the drug are effectively improved [14]. The water remediation based on the pollutant separation is an interesting area of research and porous silica found promising and potential solid materials in such remediation strategies or even used as molecular sieves to trap the polluting species from aqueous solutions [15,16].

On the other hand, rapid industrialization/urbanization has led to the serious environment concerns and caused greater ecological imbalances. An excessive discharge of industrial effluent/waste water to the natural water bodies creating several health related issues. However, a fresh and clean water supply to the society is a prime concern of related agencies [17]. Further, due to drinking of contaminated waters mankind suffered with variety of water borne diseases or even caused for death. Moreover, a survey reports that the rate of deaths raised to millions annually, mostly under the age of five, is due to the diseases transmitted through contaminated water or human excreta [17–19]. The contamination of water with heavy metal toxic ions received a greater attention in recent past because of its toxicity even at very low level [20]. Moreover, some of the heavy metals are known to be carcinogenic in nature [21]. Among the heavy metals toxic ions, lead(II) and cadmium(II) are the most toxic non-essential ions. The effluent or wastewater contaminated with these toxic ions is, therefore, be treated effectively to remove these ions completely prior to discharge it into the aquatic environment. A selective lead(II) removal was proposed using the lead(II) ion-imprinted materials based on bis-pyrazolyl functionalized mesoporous silica materials (SBA-15 or MCM-41, FDU-12). Among the synthesized materials, the Pb-IIMS-MCM-41 composite showed extremely high adsorption capacity (344.8 mg/g), fairly good selectivity and excellent reusability tested for 12 adsorption–desorption cycles [22]. In a line, selective removal of lead(II) was conducted using a grafted molecularly imprinted polymers onto hollow mesoporous silica (HMS). Relatively fast uptake of lead(II) showed fairly high adsorption capacity 40.52 mg/g and relatively high selectivity even in the presence of several heavy metal cations viz., Cu^{2+}, Zn^{2+}, Co^{2+}, Mn^{2+} and Ni^{2+} [23]. Microwave assisted hydrothermally magnetic Fe_3O_4-mesoporous magnesium silicate (FMMS) was synthesized and employed in the removal of copper(II), lead(II) and cadmium(II) from aqueous solutions. The selectivity of these heavy metals towards the solid surface FMMS followed the order Cu(II) > Pb(II) > Cd(II) [24]. The manganese

impregnated silica is found to be efficient in the remediation of water contaminated with copper(II) or lead(II) under the batch and column reactor operations. The fixed-bed studies showed that the loading capacity of column was found to be 0.190 and 0.895 mg/g for copper(II) and lead(II), respectively [25]. Similarly, iron-oxide nanoparticles immobilized silica was obtained by the wet impregnation process and employed in the low level removal of copper(II), lead(II) and cadmium(II) from aqueous solutions. Interesting to note that the sorption of copper(II) followed 'ion-exchange' along with 'inner-sphere surface complexation' mechanism whereas, cadmium(II) and lead(II) sorption predominantly followed the 'ion exchange' and electrostatic attraction by the modified silica [26]. Sericite is a natural mica-based clay employed in the efficient removal of cadmium(II) and manganese(II) from aqueous solutions [27], whereas the surface functionalized activated sericite was employed in the simultaneous removal of cadmium(II) and phenol from aqueous solutions [28]. Manganese coated sand was obtained and utilized in the removal of cadmium(II) and chromium(VI) from aqueous solutions. The manganese nanoparticles were clustered onto the sand surface which enabled it efficient materials for the selective removal of cadmium(II) and chromium(VI) from aqueous solutions at neutral pH conditions [29].

Mesoporous silica viz., MCM-48, MCM-41, HMS and SBA-15 are considered as an efficient adsorbent for water purification due to their large surface area, narrow and controlled pore size distributions [30]. Moreover, the pore sizes of silica-based porous materials are tunable from 2 to 50 nm to obtain fast responsive and highly selective material towards metal ions [31]. Several preparation methods of mesoporous silica are reported in literature; however, some methods have disadvantages due to the use of harmful chemicals that shows additional burden to the environment for its practical implications [32]. Chitosan is found to be a suitable template to form porous materials and it was used as a template for the synthesis of highly porous metal oxide microsphere [33], hybrid mesoporous sphere of aluminum and silicon oxides [34] and bimodal porous silica from rice husk [35]. In another study, the interaction of chitosan with tetraethyl orthosilicate on the formation of silica nanoparticles was explored and it was observed that the concentration of chitosan had significant influence on the size of silica nanoparticles [36]. Moreover, chitosan was employed as a template for the preparation of porous silica [37] and the three dimensional porous spinel ferrite [38] and then used for the adsorption of ibuprofen and Pb(II), respectively from aqueous solutions. Therefore, the present communication aims to obtain a mesoporous material using the chitosan and trimethoxy(octyl)silane (TMOS) as precursor materials. The thermal annealing of grafted silane with the chitosan network enabled to obtain the mesoporous chitosan-silica (M-CS) composite. The hydrophilic solid material is then employed in the efficient removal of cadmium(II) and lead(II) from aqueous solutions at various parametric studies in order to deduce the mechanism involved at solid/solution interface.

2. Materials and methods

2.1. Materials

The chitosan and TMOS (96%) are obtained from the Sigma–Aldrich, USA. Chitosan possesses medium-molecular

weight and having 75%–85% degree of deacetylation with a viscosity 20–200 cP. Glacial acetic acid, methanol and *N,N*-dimethylformamide is obtained from Merck, India. Ethanol (Analytical Reagent [AR]) is obtained from Jebsen & Jessen Gmbh & Co., Germany. Potassium dichromate (AR grade) is procured from E. Merck, Germany. The other chemicals used are of AR or equivalent grade. The water purified (18 MΩ cm) using the Millipore water purification system (Milli-Q+).

2.2. Preparation of mesoporous chitosan-silica composite

The M-CS composite was prepared by grafting the silane with chitosan network using the sol–gel synthetic route. The detailed process is described elsewhere [39] and briefly illustrated as: the chitosan is crushed in mortar and made a fine powder of it. The powder chitosan (30 g) is taken in 300 mL of *N,N*-dimethylformamide and kept in a round bottom flask. TMOS (30.52 mL) is added with dispersed chitosan. The flask is then sealed and kept in an oil bath at 105°C. The dispersion is constantly stirred for 48 h under the nitrogen atmosphere. A solution mixture of acetic acid and ethanol is added with the chitosan suspension. The amount of TMOS:acetic acid:ethanol is maintained to 1:3:6 by molar ratios. The content of the flask is further stirred for another 24 h under nitrogen atmosphere at room temperature. The gel is slowly appeared. The gel is separated from the solvents by simple centrifugation. The solid is washed repeatedly by methanol and taken in a Petri dish and kept in a drying oven at 50°C. The silane grafted chitosan was further annealed at 500°C for 3 h using electric muffle furnace (Nabertherm; Model No. LT/15/12/P330, Germany) to obtain the M-CS composite.

2.3. Characterization and surface morphology of M-CS composite

The M-CS composite is characterized by the Fourier-transform infrared (FTIR; Bruker, Tensor 27, USA, using KBR disk method) and X-ray diffraction (XRD) machine (PANalytical, Netherland; Model X'Pert PRO MPD) method. The diffraction data are recorded at a scan rate of 0.034 of 2θ illumination and at an applied voltage of 45 kV. The Cu Kα radiation is employed having the wavelength of 1.5418 Å. The surface morphology of M-CS is obtained by taking the scanning electron microscope (SEM) image and energy dispersive X-ray spectroscopy (EDX) mapping were performed by FE-SEM-Model: SU-70, Hitachi, Japan. The specific surface area, pore volume and pore size of M-CS composite are obtained by nitrogen adsorption and desorption isotherm using the Brunauer, Emmett and Teller (BET) surface area analyzer (Macsorb HM machine, Model-1201, Japan).

2.4. pH_PZC measurement

The pH_{PZC} (point of zero charge) of M-CS composite is measured using a known method [40,41]. The pH_{PZC} value is taken as the point at which the acid and base titration curves crossed the line at which $pH_{final} = pH_{initial.}$

2.5. Sorption batch experiments

Stock aqueous solutions of cadmium(II) and lead(II) (each 100.0 mg/L) are prepared by dissolving an accurate amount of cadmium(II) and lead(II) salts in purified water. The stock solutions are diluted to obtain the required cadmium(II) and lead(II) concentrations. Cadmium(II) or lead(II) solution (5.0 mg/L) is taken into polyethylene bottles and the pH of these solutions is adjusted to the required pH by dropwise addition of concentrated HCl/NaOH. M-CS solid (0.1 g) is then taken into these bottles contained with cadmium(II) or lead(II) solution. The bottles are sealed properly using parafilm and placed in an automatic incubator shaker (TM Weiber, ACMAS Technologies Pvt. Ltd., India) for 24 h at 25°C. A prolonged period is given to achieve an apparent equilibrium between the solid/solution interfaces. The bottle samples are taken out from the shaker and solutions are filtered with 0.45 μm syringe filter. The pH of filtrate is again monitored and reported as equilibrium pH. The filtrates are subjected to obtain the final concentration (i.e., after adsorption) of lead(II) or cadmium(II) using microwave plasma-atomic emission spectrometry (MP-AES; Agilent Technologies, Model 4200 MP-AES). Similarly, the initial concentration of cadmium(II) or lead(II) is also measured using the MP-AES. Therefore, using the initial and final concentrations of cadmium(II) or lead(II) the percentage removal of cadmium(II) or lead(II) is calculated.

Similar sorption process is adopted for sorptive concentration dependence studies. The concentration of cadmium(II) or lead(II) is varied from ~5.0 to 50.0 at pH ~5.0. The results are presented as percentage of cadmium(II) or lead(II) removal as a function of initial sorptive concentrations.

The equilibrium stage concentration dependence sorption data are then modelled to the linear equation of the Langmuir and Freundlich adsorption isotherm models. The linearized Langmuir adsorption isotherm [42] is employed as given in Eq. (1):

$$\frac{C_e}{q} = \frac{1}{q_m K_L} + \frac{C_e}{q_m} \tag{1}$$

where q is the amount of cadmium(II) or lead(II) adsorbed per unit weight of M-CS solid (mg/g) at equilibrium; C_e is the equilibrium bulk sorbate concentration (mg/L); q_m is the Langmuir monolayer adsorption capacity, that is, the amount of solute required to occupy all the available sites in unit mass of solid sample (mg/g) and K_L is the Langmuir constant (L/g).

Furthermore, a linear form of Freundlich isotherm [42] (Eq. (2)) is used to deduce the Freundlich constants in the sorption of cadmium(II) or lead(II) by M-CS solid.

$$\log q = \frac{1}{n}\log C_e + \log K_f \tag{2}$$

where q and C_e are the amount adsorbed (mg/g) and bulk sorbate concentration (mg/L) at equilibrium, respectively. K_f and $1/n$ are the Freundlich constants referring to the adsorption capacity and adsorption intensity or surface heterogeneity of solid, respectively.

The background electrolyte dependence sorption of cadmium(II) by the M-CS composite is performed varying the background electrolyte concentration of sorptive solutions from 0.0001 to 0.1 mol/L NaNO_3. The solution pH ~5.0 is adjusted and sorption experiments are conducted at constant temperature 25°C. The results are presented as the percentage

of cadmium(II) removed against the background electrolyte concentrations.

The efficiency of M-CS solid at least in the removal of cadmium(II) or lead(II) is assessed performing the time dependence sorption studies. The time dependence studies for the sorption of cadmium(II) and lead(II) by the M-CS composite is carried out at an initial concentration of cadmium(II) or lead(II) 5.0 mg/L, pH ~5.0 and at 25°C. The results are presented as the amount of cadmium(II) or lead(II) removed (mg/g) as a function of time (min). The time dependence sorption data are then employed to deduce the kinetic modelling studies hence, to obtain the rate constant values and the capacity of M-CS solid for cadmium(II) or lead(II). Three different kinetic models viz., the pseudo-first-order (PFO) [43], pseudo-second-order (PSO) [43] and fractal-like pseudo-second-order (FL-PSO) [44] models to its non-linear form, that is, Eqs. (3)–(5), respectively, are utilized for the studies.

$$q_t = q_e \left(1 - e^{-k_1 t}\right) \tag{3}$$

$$q_t = q_e \frac{q_e k_2 t}{1 + q_e k_2 t} \tag{4}$$

$$q_t = \frac{k q_e^2 t^\alpha}{1 + k q_e t^\alpha} \tag{5}$$

where q_t and q_e are the amounts of cadmium(II) or lead(II) adsorbed at time t and the adsorption capacity at equilibrium, respectively. k_1 and k_2 are the PFO and PSO rate constants, respectively. The constants k and α are the rate constant and the fractal constant, respectively.

2.6. Column experiments

A fixed-bed column study is conducted employing a glass column of 30 cm long having inner diameter 1 cm. 0.5 g of M-CS solid is packed in the middle of column, and rest of the column is packed with glass beads. Cadmium(II) or lead(II) solution (~5.0 mg/L; pH ~5.5) is pumped upward from the bottom of the column using peristaltic pump (KrosFlo Research I Peristaltic Pump, Spectrum Laboratories Inc., CA, USA) at a constant flow rate of 1.0 mL/min. The effluent samples are collected using a fraction collector (Spectra/Chrom CF-2 Fraction Collector, Spectrum Laboratories). The liquid samples collected are filtered using a 0.45 μm syringe filter and the total bulk sorbate concentration is measured using the MP-AES. The results are presented as a fraction concentration of cadmium(II) or lead(II) (i.e., C_e/C_0; where the C_0 and C_e are the concentrations (mg/L) of the influent and effluent cadmium(II) or lead(II) solution, respectively) against the throughput volume.

The breakthrough data are simulated to known Thomas equation (Eq. (6)) [45] in order to obtain the loading capacity of M-CS composite for cadmium(II) under the dynamic conditions.

$$\frac{C_e}{C_0} = \frac{1}{1 + e^{\left[K_T\left(q_0 m - C_0 V\right)\right]/Q}} \tag{6}$$

where K_T is the Thomas rate constant (L/min/mg); q_0 is the maximum amount of the cadmium(II) or lead(II) that loaded (mg/g) under the specified column conditions; m is the mass of M-CS solid (g) taken in the column, V is the throughput volume (L) and Q is the flow rate of the pumped sorptive solution (L/min). A non-linear regression of the breakthrough data are conducted by the least square fitting method and optimized the values for the two unknown parameters (K_T and q_0). For the purpose the Microsoft Excel add-ins 'Solver' is employed with user-defined functions to minimize the residuals between the model-calculated and model-measured values.

3. Results and discussion

3.1. Characterization M-CS composite

The FTIR spectrum of chitosan, TMOS grafted chitosan and M-CS composite is shown in Fig. 1. It is to be noted that the characteristic peak corresponding to N–H vibration appeared at 1,592 cm⁻¹ in chitosan sample was shifted to 1,558 cm⁻¹ after the chitosan was grafted with TMOS. This result supported the bonding of silane with the amino group of chitosan [46]. It is clearly to be observed that several bands disappeared in FTIR graph of M-CS composite and the two dominant peaks at the wave numbers around 1,030 and 772 cm⁻¹ correspond to the asymmetric and symmetric vibrations of Si–O–Si, respectively [47,48]. Moreover, an additional peak that occurred around 1,610 cm⁻¹ is perhaps due to the carbonyl group possibly present in M-CS composite [46]. The peak corresponds to the silanol group is not clearly identified from the FTIR spectrum which is perhaps due to overlapping with asymmetric stretching peaks of Si–O–Si.

A SEM micrograph of M-CS composite is presented in Fig. 2. Some macropores are visible and they are unevenly distributed on the M-CS surface. It is difficult to see the mesopores of M-CS from SEM images; therefore, BET method is applied to determine the pore size and pore volume. The EDX mapping is conducted with the M-CS sample and the results are shown in Fig. 3. It clearly shows that the M-CS
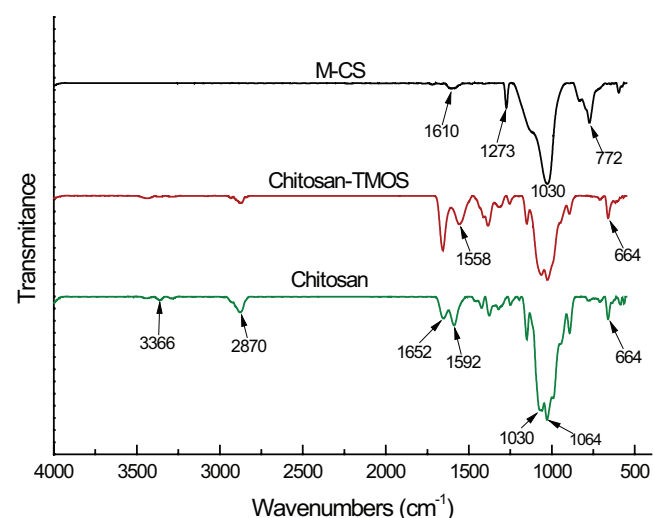
Fig. 1. FTIR spectra of chitosan, trimethoxy(octyl)silane grafted chitosan and M-CS composite.
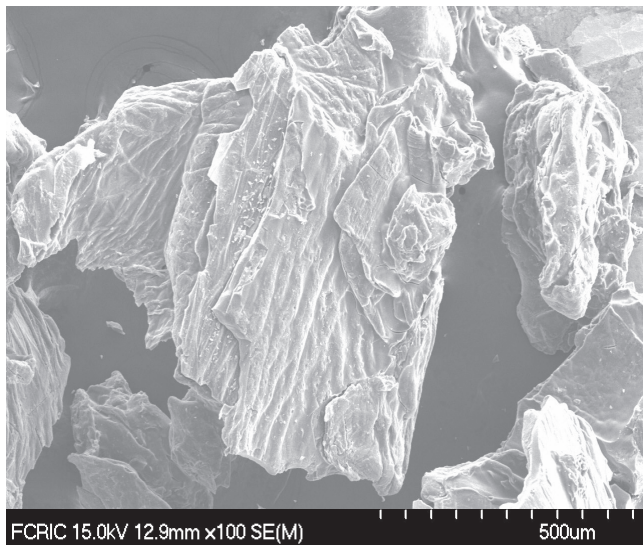
Fig. 2. SEM image of M-CS composite.
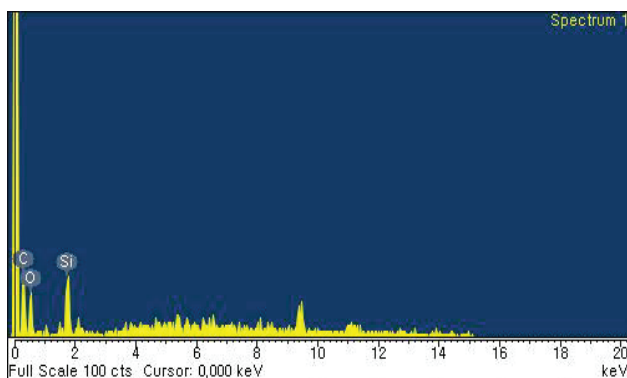
Fig. 3. EDX mapping of M-CS composite.

solid is possessed with a strong peak of silicon indicated the sample is contained with silica.

XRD data are obtained for the M-CS solid and results are illustrated in Fig. 4. A predominant reflection occurred at around 2θ value of 23.13° is due to the presence of silica in these samples. Further, XRD pattern obtained indicates that the M-CS solid possesses more amorphous in nature.

The BET specific surface area along with pore size and pore volume of M-CS is obtained and the N_2 adsorption and desorption results are shown in Fig. 5(a). The IUPAC classification indicated that the Type IV adsorption isotherm is characterized to the mesoporous materials having the pore diameter between 2 and 50 nm [49]. The M-CS solid clearly shows a H4 type hysteresis loop, showing adsorption desorption branches parallel and nearly horizontal, this indicates that the solid possesses a narrow slit-shaped pores, contained with some microporosity [50]. The specific surface area obtained for M-CS composite is 371.77 m^2/g. Moreover, the pore size distribution curve is shown in Fig. 5(b). The average pore diameter is 3.62 nm and average pore volume is 0.065 cm^3/g, respectively. This clearly indicated that the synthesized M-CS composite is possessed with mesopores on its surface. Additionally, the pH_{PZC} value of M-CS composite is also measured and found to be 6.75.
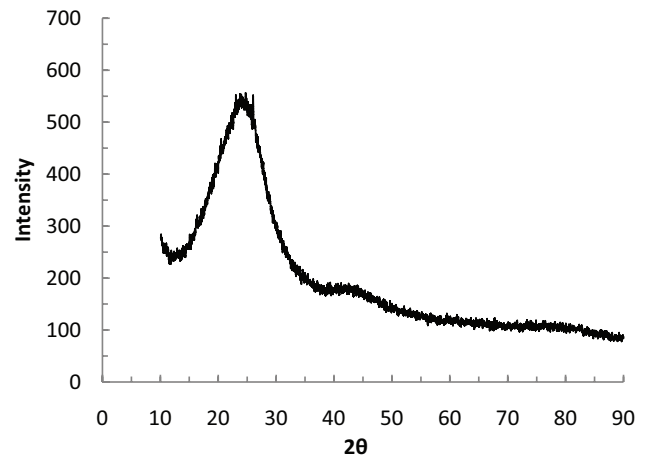
Fig. 4. X-ray diffraction pattern for M-CS composite.
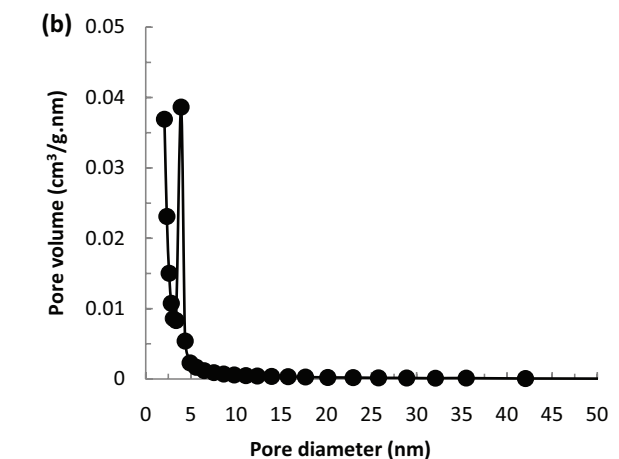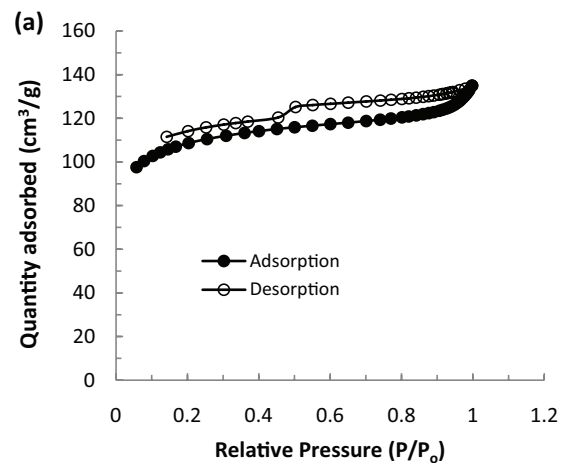
Fig. 5. (a) Nitrogen adsorption–desorption isotherm and (b) pore size distribution curve of M-CS composite.

3.2. Batch studies

3.2.1. Effect of solution pH

The M-CS solid is further employed in the remediation of water contaminated with two important heavy metal

toxic ions viz., cadmium(II) and lead(II). The pH dependence removal is an important parameter enabled to study the mechanistic aspects of sorption process since the surface properties of solid and the speciation of sorbate ions are greatly influenced with the change in solution pH. Therefore, systematic pH dependence sorption of cadmium(II) and lead(II) by the M-CS composite is conducted varying the initial pH from 2.0 to 10.0. As shown in Fig. 6, the uptake of cadmium(II) or lead(II) is sharply increased with a gradual and steady increase of solution pH. At moderate pH value (i.e., pH ~6.0), it attained almost a 100% removal of these two ions by M-CS solid. The uptake of cadmium(II) is increased from 0.20% to 100.0% with the increase in pH from 2.34 to 7.37, respectively. Similarly, increasing the pH from 2.43 to 7.47 the corresponding increase in lead(II) uptake is found to be from 0.21% to 100.0%. The pH dependence behaviour of cadmium(II) and lead(II) is ascribed by the speciation studies of cadmium(II) and lead(II) as well as the pH dependence surface properties of solid. The acid–base titrations conducted separately show that the M-CS solid possessed pH_{PZC} at pH 6.75. This indicates that the surface possesses net positive charge below to this pH and net negative charge above to this pH. The acid/base dissociation/association could be represented as Eq. (7):

$$\equiv M - CS - OH_2^+ \leftrightarrow \equiv M - CS - OH^0 \leftrightarrow \equiv M - CS - O^- \atop pH_{PZC} \tag{7}$$
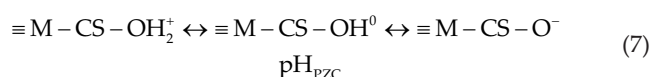
The speciation studies conducted for the cadmium(II) and lead(II) stated that until pH 8.8 the cadmium(II) exists as cationic species Cd^{2+} and beyond this pH it predominantly turns into the insoluble $Cd(OH)_2(S)$ species. In between an insignificant percentage (*ca.* 5%) of $Cd(OH)^+$ species occurred at around pH 8.7. Therefore, within the studied pH the cadmium(II) is predominantly present as cationic species only. On the other hand, lead(II) exists as cationic species Pb^{2+} up until the pH 6.2 and above to this pH, it turns mainly into insoluble $Pb(OH)_2(S)$ species. Similar to cadmium(II), an insignificant soluble species $Pb(OH)^+$ is present (maximum *ca.* 5%) at pH 6.1 [26]. A low percentage uptake of cadmium(II) and

lead(II) by M-CS composite at low pH values is ascribed due to the two factors (i) both the solid surface and sorbate ions are possessed with net positive charges which lead to a strong electrostatic repulsion that restricts the metal cations to enter into the Stern layer and proceed for binding onto the surface active sites. (ii) At low pH conditions an excess of positively charged hydrogen ions (H^+) may compete for the active surface sites with a greater mobility of ions which further restricts the uptake of these cations by the M-CS solid. A similar observation was viewed in the removal of lead(II) using various modified mesoporous silica materials [22] or the removal of cadmium(II) by activated biochar [51].

Further, a gradual increase in pH leads to the increase in percentage uptake of cadmium(II) or lead(II) by M-CS solid. This is due to the acidic dissociation of solid surface that causes a gradual increase in negative surface charge that eventually attracts the cationic species of cadmium(II) and lead(II) towards the solid surface and an enhanced uptake of these two ions occurs (pH_{PZC} is 6.75). It is observed that at pH 5.27 for lead(II) or 5.67 for cadmium(II), almost 100% removal of these cations is occurred that shows strong affinity of cadmium(II) and lead(II) towards the M-CS solid. The results further indicate that an electrostatic attraction of cadmium(II) and lead(II) by the M-CS solid enables these cations to enter within the Stern layer and allows them to form an inner sphere complexes on to the solid surface. This, perhaps, forms relatively the strong chemical bonds between the metal cations and active surface silanol group of M-CS composite [52,53].

3.2.2. Effect of cadmium(II) and lead(II) concentrations

The concentration dependence sorption of cadmium(II) and lead(II) by the M-CS solid is conducted at a wide range of initial sorbate concentrations, that is, from 6.41 to 51.68 mg/L at a constant equilibrium pH ~5.5 for cadmium(II) and pH ~5.0 for lead(II) at a constant sorbent dose of 2.0 g/L and temperature 25°C. The equilibrium stage percentage removal of cadmium(II) and lead(II) against the initial concentration of sorbate ions by the M-CS composite is illustrated in Fig. 7. It is evident that increasing the initial concentration of sorbate ions eventually caused to decrease the percentage removal
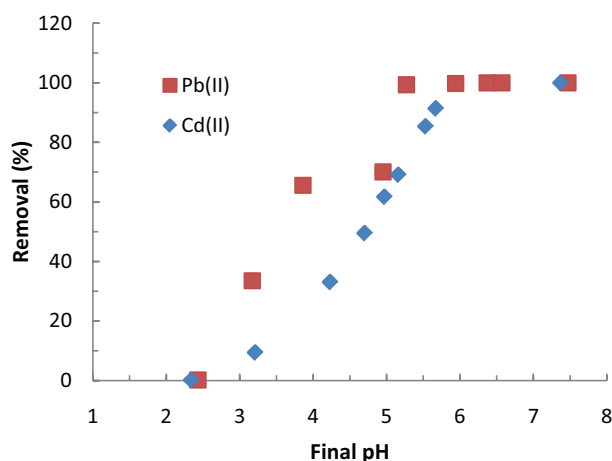
Fig. 6. Effect of pH in the removal of cadmium(II) and lead(II) using M-CS composite.
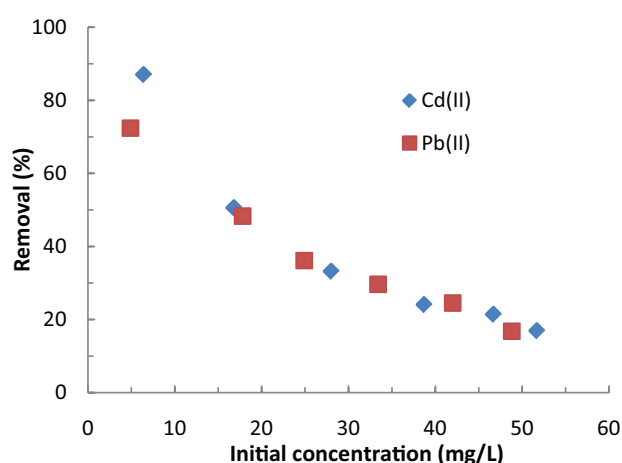
Fig. 7. Percentage removal of cadmium(II) and lead(II) at various initial concentrations of sorptive solutions by M-CS composite.

of these two cations by M-CS solid. Quantitatively, increasing the concentration of cadmium(II) from 6.41 to 51.68 mg/L caused to a corresponding decrease in percentage removal of cadmium(II) from 87.05% to 16.93%. Similarly, increasing the lead(II) concentration from 4.50 to 48.80 mg/L caused to a decrease in percentage of lead removal from 72.39% to 16.80% by the M-CS solid. A decrease in percentage removal of cadmium(II) or lead(II) at an increased initial concentration of these metal ions by the M-CS solid is explicable by the fact that relatively more number of active sites are available onto the solid surface for lesser number of sorbate ions at lower sorbate concentration. Whereas increasing the sorbate concentrations at the same solid dose, relatively lesser number of active sites are available for enhanced number of sorbate species which results in decrease of percentage removal of sorbate ions [54,55]. However, a similar increase in sorbate ion concentrations (cadmium(II) or lead(II)) has led to an apparent increase in amount adsorbed by M-CS composite (data not shown). Similar increase of phthalate esters uptake was occurred while increasing the phthalate ester initial concentrations using the phenyl-functionalized mesoporous silica material as sorbent [1]. Results show the affinity of surface active sites of M-CS towards the cadmium(II) and lead(II) which apparently indicates the potential use of M-CS composite in the remediation of water contaminated with cadmium(II) or lead(II).

3.2.3. Adsorption isotherm models

The equilibrium stage sorption data for cadmium and lead(II) are attempted to fit with the linearized Langmuir and Freundlich adsorption isotherm models (Eqs. (1) and (2)). The fitting results are given in Table 1. The results clearly indicate that the sorption data for cadmium(II) and lead(II) are fitted relatively well to the Langmuir adsorption model than the Freundlich model since the correlation coefficient (R^2) is relatively high for the Langmuir model fitting. The values of Langmuir constants, that is, Langmuir monolayer sorption capacity (q_m) and Langmuir rate constant (K_L) are estimated, along with the R^2 values for cadmium(II) and lead(II) and presented in Table 1. The high value of q_m obtained for cadmium(II) and lead(II) by the M-CS composite shows the affinity of solid towards the cadmium(II) and lead(II). This further indicates the potential use of solid in the removal of these two pollutants from aqueous solutions. Further, the applicability of Langmuir adsorption isotherm pointed that the surface active sites are distributed evenly onto the surface. Although the adsorption data are relatively less fitted to the Freundlich adsorption isotherm; however, the estimated Freundlich constants along with the R^2 values are obtained for the sorption of cadmium(II) and lead(II) by M-CS composite and shown in Table 1.

3.2.4. Effect of background electrolyte concentrations

The background electrolyte concentration is an important parameter to understand the sorption mechanism. The specific sorption having strong chemical forces are usually not affected significantly by increasing the background electrolyte concentrations; however, the non-specific sorption with weaker electrostatic or physical forces are greatly influenced with an increase in background electrolyte concentrations [39,56]. Therefore, the sorption study is extended varying the background electrolyte concentrations from 0.0001 to 0.1 mol/L NaNO$_3$. The results are presented with the percentage of cadmium(II) removal as a function of background electrolyte concentrations and shown in Fig. 8. It is observed that increasing the background electrolyte concentrations from 0.0001 to 0.1 mol/L (1,000 times increase) is only caused to decrease the percentage uptake of cadmium(II) from 81.88% to 59.70% (i.e., 22.18% decrease) by the M-CS solid. This indicates that the 1,000 times increase in background electrolyte concentrations does not affect significantly the percentage removal of cadmium(II). Therefore, this eventually concludes that the sorbate ions are forming an 'inner sphere complexes' with strong chemical forces onto the solid surface. It was previously reported that the uptake of EE2 (17α-ethynyl estradiol) and tetracycline are not affected increasing the NaCl concentrations from the 0.0001 to 0.1 mol/L by several hybrid materials precursor to the natural clay [57].

3.2.5. Kinetic studies

The time dependence sorption enables the efficiency of material in the removal of pollutants from aqueous solutions
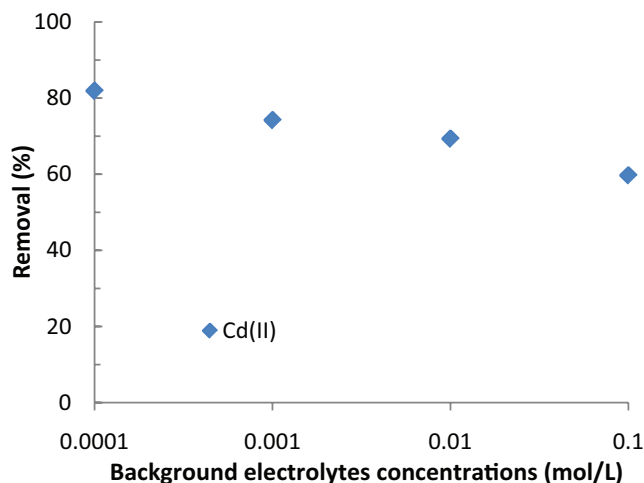
Fig. 8. Effect of background electrolytes concentrations in the removal of cadmium(II) by M-CS composite.

Table 1
Langmuir and Freundlich constants obtained for the sorption of cadmium(II) and lead(II) by M-CS composite

	Langmuir model			Freundlich model		
	q_m (mg/g)	K_L (L/g)	R^2	$1/n$	K_f (mg/g)	R^2
Cadmium(II)	5.208	2.943	0.988	0.120	3.034	0.866
Lead(II)	4.587	0.376	0.961	0.288	1.845	0.814

and paves the way to deduce the kinetics of sorption in the solid materials. Therefore, the time dependence sorption of cadmium(II) and lead(II) by M-CS solid is conducted by varying the time of contact from 1 to 180 min for cadmium(II) and 1 to 240 min for lead(II) keeping a constant initial pollutant concentration 5.0 mg/L. The time dependence sorption of cadmium(II) and lead(II) as a function of time is presented in Figs. 9(a) and (b). A very fast initial uptake of cadmium(II) and lead(II) occurred which attain an apparent saturation within a lapse of time *ca*. 120 min (for cadmium(II)) and 60 min (for lead(II)). This indicates that the M-CS composite shows a strong affinity towards these two heavy metal toxic ions, and within a short period of time an apparent equilibria is achieved between the solid/solution interface.

Further, the time dependence uptake of cadmium(II) and lead(II) is employed to perform the kinetic modelling using three different kinetic models viz., PFO, PSO and FL-PSO as stated in Eqs. (3)–(5), respectively. A non-linear least square fitting is conducted to optimize the unknown parameters and the fitting curves are shown in Figs. 9(a) and (b) with dotted lines. Moreover, the estimated unknown parameters

along with the least square sum are presented in Table 2. The results clearly indicate that time dependence uptake of cadmium(II) and lead(II) is relatively fitted well to the non-linear PSO and FL-PSO models compared to the PFO model since the least square sum is found reasonably low for PSO and FL-PSO models. The applicability of PSO or FL-PSO indicates that the sorbate species are aggregated onto the solid surface with relatively strong chemical forces [58]. Moreover, the M-CS composite possesses almost an identical removal capacity for cadmium(II) and lead(II) under the specified experimental conditions.

3.3. Fixed-bed column studies

The removal of cadmium(II) by M-CS composite under the dynamic conditions is assessed under the fixed-bed column reactor experiments. The column conditions are maintained as described before. The column reactor data are shown in Fig. 10. It is evident from the breakthrough curve

Table 2
Estimated kinetic parameters for the PFO, PSO and FL-PSO kinetic models in the sorption of cadmium(II) and lead(II) by M-CS composite

Models	Constants estimated	Cd(II)	Pb(II)
PFO	q_e (mg/g)	2.128	1.516
	k_1 (min^{-1})	0.191	0.0215
	s^2	0.648	0.169
PSO	q_e (mg/g)	2.252	1.816
	k_2 (g/mg/min)	0.141	0.0135
	s^2	0.272	0.16
FL-PSO	q_e (mg/g)	3.347	3.785
	k (g/mg/min)	0.111	0.013
	α	0.365	0.493
	s^2	0.006	0.109

s^2: Least square sum.
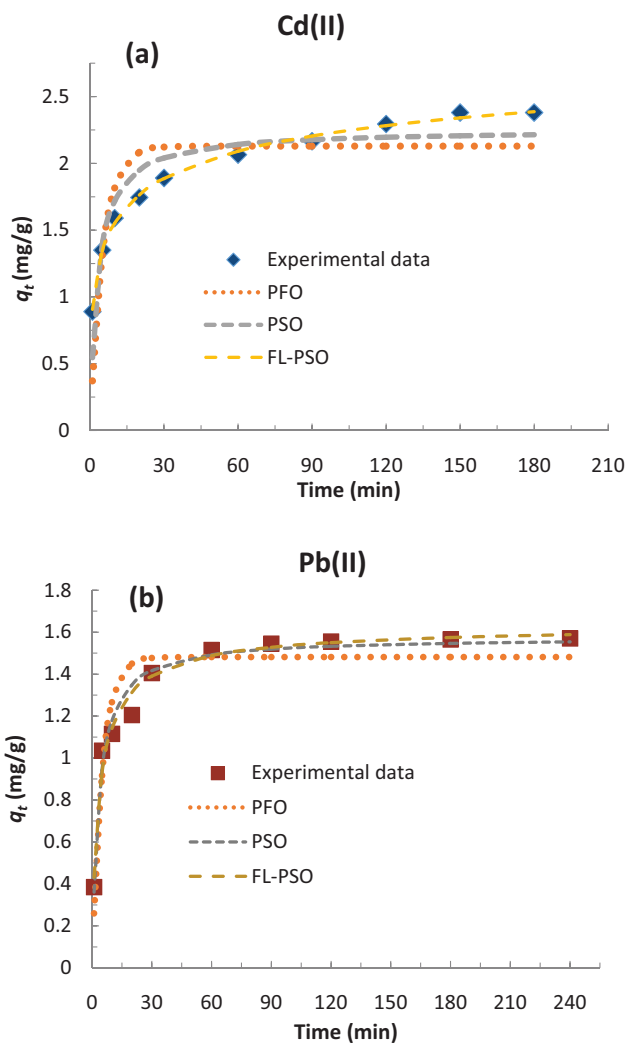
Fig. 9. Time dependence uptake of (a) cadmium(II) and (b) lead(II) by M-CS composite.
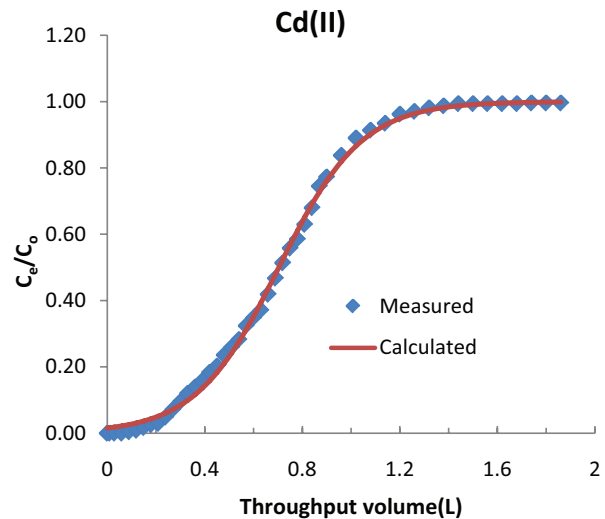
Fig. 10. Breakthrough curve obtained for cadmium(II) removal by M-CS composite.

(Fig. 10) that a complete breakthrough is obtained at the throughput volume of 1.53 L. A high value of breakthrough volume obtained for cadmium(II) further indicated the strong affinity of M-CS solid towards the cadmium(II). Moreover, a non-linear fitting is conducted using the Thomas equation (Eq. (6)). The fitting curve is shown in Fig. 10. The breakthrough data are fitted well to the Thomas model. Further, the Thomas constants, that is, loading capacity and Thomas rate constant are estimated and found to be 11.65 mg/g and 8.57×10^{-4} L/min/mg, respectively, with a least square sum of 5.0×10^{-2}. Interesting to note that a marked increase in removal capacity of cadmium(II) by the M-CS composite is obtained using the fixed-bed column reactor studies compared to the batch studies. This is due to the fact that the sorbing species are allowed to give prolong and continuous contact time with the solid surface which results a complete exhaustion of solid and giving out an enhanced removal capacity [53]. A high loading of cadmium(II) by M-CS composite shows an enhanced utility of material in the large scale/pilot plant level utilization of material in the remediation of aquatic environment contaminated with cadmium under the column reactor operations.

4. Conclusion

The M-CS composite was obtained using the precursor materials chitosan and TMSO. The TMOS was initially grafted with chitosan polymer and annealed at 500°C to obtain a composite material. The BET specific surface area and pore size of the solid was found to be 371.77 m^2/g and 3.62 nm, respectively. XRD data showed more amorphous nature of the solid. The FTIR analysis indicated the presence of Si–O–Si condensed silica network. The M-CS composite was then employed in the removal of cadmium(II) and lead(II) from aqueous solutions under the batch and column reactor studies. Increase in solution pH and sorbate concentrations greatly favoured the uptake of cadmium(II) and lead(II) from aqueous solutions. At around neutral pH, almost 100% removal of these two ions was achieved by the M-CS solid. The concentration dependence data were fitted well to the Langmuir adsorption model compared with the Freundlich model. Langmuir monolayer adsorption capacity of M-CS composite was estimated to be 5.208 and 4.587 mg/g for the cadmium(II) and lead(II), respectively. Relatively a fast initial uptake of cadmium(II) and lead(II) by M-CS composite attained an apparent equilibrium within 120 and 60 min of contact for cadmium and lead, respectively. Moreover, the kinetic data were fitted well to the PSO and FL-PSO kinetic models. The 1,000 times increase in background electrolyte concentrations ($NaNO_3$) did not affect significantly the percentage removal of cadmium(II) by the M-CS solid which indicated that the polluting ions were forming an inner-sphere complexes with relatively stronger chemical forces onto the solid surface. A high breakthrough volume was obtained and the breakthrough data were fitted well to the Thomas equation. The estimated loading capacity for cadmium(II) by M-CS composite was found to be 11.65 mg/g. Overall, the results indicated that M-CS composite is found to be an efficient and promising solid to be employed for the effective remediation of water contaminated with cadmium(II) and lead(II).

References

[1] J. Fan, X. Wang, W. Teng, J. Yang, X. Ran, X. Gou, N. Bai, M. Lv, H. Xu, G. Li, W. Zhang, D. Zhao, Phenyl-functionalized mesoporous silica materials for the rapid and efficient removal of phthalate esters, J. Colloid Interface Sci., 487 (2017) 354–359.

[2] B. Kumar, S. Kulanthaivel, A. Mondal, S. Mishra, B. Banerjee, A. Bhaumik, I. Banerjee, S. Giri, Mesoporous silica nanoparticle based enzyme responsive system for colon specific drug delivery through guar gum capping, Colloids Surf., B, 150 (2017) 352–361.

[3] Y. Wang, Q. Zhao, N. Han, L. Bai, J. Li, J. Liu, E. Che, L. Hu, Q. Zhang, T. Jiang, S. Wang, Mesoporous silica nanoparticles in drug delivery and biomedical applications, Nanomed. Nanotechnol. Biol. Med., 11 (2015) 313–327.

[4] Z. Tian, Y. Xu, Y. Zhu, Aldehyde-functionalized dendritic mesoporous silica nanoparticles as potential nanocarriers for pH-responsive protein drug delivery, Mater. Sci. Eng., C, 71 (2017) 452–459.

[5] G. Xue, F. Yurun, M. Li, G. Dezhi, J. Jie, Y. Jincheng, S. Haibin, G. Hongyu, Z. Yujun, Phosphoryl functionalized mesoporous silica for uranium adsorption, Appl. Surf. Sci., 402 (2017) 53–60.

[6] Q. Gao, H. Li, Y. Ling, B. Han, K. Xia, C. Zhou, Synthesis of $MnSiO_3$ decorated hollow mesoporous silica spheres and its promising application in environmental remediation, Microporous Mesoporous Mater., 241 (2017) 409–417.

[7] R. Malik, P.S. Rana, V.K. Tomer, V. Chaudhary, S.P. Nehra, S. Duhan, Nano gold supported on ordered mesoporous WO_3/ SBA-15 hybrid nanocomposite for oxidative decolorization of azo dye, Microporous Mesoporous Mater., 225 (2016) 245–254.

[8] H. Zhao, T. Zhang, J. Dai, K. Jiang, T. Fei, Preparation of hydrophilic organic groups modified mesoporous silica materials and their humidity sensitive properties, Sens. Actuators, B, 240 (2017) 681–688.

[9] J.M. Falcón, L.M. Otubo, I.V. Aoki, Highly ordered mesoporous silica loaded with dodecylamine for smart anticorrosion coatings, Surf. Coat. Technol., 303 (2016) 319–329.

[10] S.-H. Lim, E.-J. Woo, H. Lee, C.-H. Lee, Synthesis of magnetite–mesoporous silica composites as adsorbents for desulfurization from natural gas, Appl. Catal., B, 85 (2008) 71–76.

[11] F. Chen, R. Shi, Y. Xue, L. Chen, Q.-H. Wan, Templated synthesis of monodisperse mesoporous maghemite/silica microspheres for magnetic separation of genomic DNA, J. Magn. Magn. Mater., 322 (2010) 2439–2445.

[12] S.-H. Wu, Y.-S. Lin, Y. Hung, Y.-H. Chou, Y.-H. Hsu, C. Chang, C.-Y. Mou, Multifunctional mesoporous silica nanoparticles for intracellular labeling and animal magnetic resonance imaging studies, Chem. Biochem., 9 (2008) 53–57.

[13] J. Gañán, S. Morante-Zarcero, D. Pérez-Quintanilla, I. Sierra, Evaluation of mesoporous imprinted silicas as MSPD selective sorbents of ketoprofen in powder milk, Mater. Lett., 197 (2017) 5–7.

[14] Y. Bi, C. Wu, M. Xin, S. Bi, C. Yan, J. Hao, F. Li, S. Li, Facile large-scale preparation of mesoporous silica microspheres with the assistance of sucrose and their drug loading and releasing properties, Int. J. Pharm., 500 (2016) 77–84.

[15] X. Zhao, Y. Shi, T. Wang, Y. Cai, G. Jiang, Preparation of silica-magnetite nanoparticle mixed hemimicelle sorbents for extraction of several typical phenolic compounds from environmental water samples, J. Chromatogr., A, 1188 (2008) 140–147.

[16] M. Brigante, E. Pecini, M. Avena, Magnetic mesoporous silica for water remediation: synthesis, characterization and application as adsorbent of molecules and ions of environmental concern, Microporous Mesoporous Mater., 230 (2016) 1–10.

[17] M.A. Montgomery, M. Elimelech, Water and sanitation in developing countries: including health in the equation, Environ. Sci. Technol., 41 (2007) 17–24.

[18] N.J. Ashbolt, Microbial contamination of drinking water and disease outcomes in developing regions, Toxicology, 198 (2004) 229–238.

[19] N.J. Ashbolt, Microbial contamination of drinking water and human health from community water systems, Curr. Environ. Health Rep., 2 (2015) 95–106.

[20] E. Alipanahpour Dil, M. Ghaedi, G.R. Ghezelbash, A. Asfaram, M.K. Purkait, Highly efficient simultaneous biosorption of Hg²⁺, Pb²⁺ and Cu²⁺ by live yeast *Yarrowia lipolytica* 70562 following response surface methodology optimization: kinetic and isotherm study, J. Ind. Eng. Chem., 48 (2017) 162–172.

[21] M. Hossein Beyki, M.H. Ghasemi, A. Jamali, F. Shemirani, A novel polylysine–resorcinol base γ-alumina nanotube hybrid material for effective adsorption/preconcentration of cadmium from various matrices, J. Ind. Eng. Chem., 46 (2017) 165–174.

[22] H.-Z. Cui, Y.-L. Li, S. Liu, J.-F. Zhang, Q. Zhou, R. Zhong, M.-L. Yang, X.-F. Hou, Novel Pb(II) ion-imprinted materials based on bis-pyrazolyl functionalized mesoporous silica for the selective removal of Pb(II) in water samples, Microporous Mesoporous Mater., 241 (2017) 165–177.

[23] Z. Zhang, X. Zhang, D. Niu, Y. Li, J. Shi, Highly efficient and selective removal of trace lead from aqueous solutions by hollow mesoporous silica loaded with molecularly imprinted polymers, J. Hazard. Mater., 328 (2017) 160–169.

[24] Z. Zhao, X. Zhang, H. Zhou, G. Liu, M. Kong, G. Wang, Microwave-assisted synthesis of magnetic Fe₃O₄-mesoporous magnesium silicate core-shell composites for the removal of heavy metal ions, Microporous Mesoporous Mater., 242 (2017) 50–58.

[25] D. Tiwari, C. Laldanwngliana, C.-H. Choi, S.M. Lee, Manganese-modified natural sand in the remediation of aquatic environment contaminated with heavy metal toxic ions, Chem. Eng. J., 171 (2011) 958–966.

[26] S.-M. Lee, C. Laldawngliana, D. Tiwari, Iron oxide nano-particles-immobilized-sand material in the treatment of Cu(II), Cd(II) and Pb(II) contaminated waste waters, Chem. Eng. J., 195–196 (2012) 103–111.

[27] S.M. Lee, Lalhmunsiama, D. Tiwari, Sericite in the remediation of Cd(II)- and Mn(II)-contaminated waters: batch and column studies, Environ. Sci. Pollut. Res. Int., 21 (2014) 3686–3696.

[28] Lalhmunsiama, D. Tiwari, S.-M. Lee, Surface-functionalized activated sericite for the simultaneous removal of cadmium and phenol from aqueous solutions: mechanistic insights, Chem. Eng. J., 283 (2016) 1414–1423.

[29] S.-M. Lee, W.-G. Kim, C. Laldawngliana, D. Tiwari, Removal behavior of surface modified sand for Cd(II) and Cr(VI) from aqueous solutions, J. Chem. Eng. Data, 55 (2010) 3089–3094.

[30] E. Da'na, Adsorption of heavy metals on functionalized-mesoporous silica: a review, Microporous Mesoporous Mater., 247 (2017) 145–157.

[31] C.-H. Zhang, G.-J. Li, J.-H. Wang, Application of nanopore and porous materials for heavy metal ion detection, Chin. J. Anal. Chem., 42 (2014) 607–615.

[32] A.B.D. Nandiyanto, S.-G. Kim, F. Iskandar, K. Okuyama, Synthesis of spherical mesoporous silica nanoparticles with nanometer-size controllable pores and outer diameters, Microporous Mesoporous Mater., 120 (2009) 447–453.

[33] A.E. Kadib, K. Molvinger, T. Cacciaguerra, M. Bousmina, D. Brunel, Chitosan templated synthesis of porous metal oxide microspheres with filamentary nanostructures, Microporous Mesoporous Mater., 142 (2011) 301–307.

[34] T.P. Braga, E.C.C. Gomes, A.F. de Sousa, N.L.V. Carreño, E. Longhinotti, A. Valentini, Synthesis of hybrid mesoporous spheres using the chitosan as template, J. Non-Cryst. Solids, 355 (2009) 860–866.

[35] T. Witoon, M. Chareonpanich, J. Limtrakul, Synthesis of bimodal porous silica from rice husk ash via sol–gel process using chitosan as template, Mater. Lett., 62 (2008) 1476–1479.

[36] T. Witoon, M. Chareonpanich, Interaction of chitosan with tetraethyl orthosilicate on the formation of silica nanoparticles: effect of pH and chitosan concentration, Ceram. Int., 38 (2012) 5999–6007.

[37] T. Numpilai, S. Muenmee, T. Witoon, Impact of pore characteristics of silica materials on loading capacity and release behavior of ibuprofen, Mater. Sci. Eng., C, 59 (2016) 43–52.

[38] D.H.K. Reddy, S.-M. Lee, Three-dimensional porous spinel ferrite as an adsorbent for Pb(II) removal from aqueous solutions, Ind. Eng. Chem. Res., 52 (2013) 15789–15800.

[39] Lalhmunsiama, Lalchhingpuii, B.P. Nautiyal, D. Tiwari, S.I. Choi, S.-H. Kong, S.-M. Lee, Silane grafted chitosan for the

[40] J. Rivera-Utrilla, I. Bautista-Toledo, M.A. Ferro-García, C. Moreno-Castilla, Activated carbon surface modifications by adsorption of bacteria and their effect on aqueous lead adsorption, J. Chem. Technol. Biotechnol., 76 (2001) 1209–1215.

[41] Lalhmunsiama, S.M. Lee, D. Tiwari, Manganese oxide immobilized activated carbons in the remediation of aqueous wastes contaminated with copper(II) and lead(II), Chem. Eng. J., 225 (2013) 128–137.

[42] R.R. Pawar, Lalhmunsiama, H.C. Bajaj, S.-M. Lee, Activated bentonite as a low-cost adsorbent for the removal of Cu(II) and Pb(II) from aqueous solutions: batch and column studies, J. Ind. Eng. Chem., 34 (2016) 213–223.

[43] D. Balarak, E. Bazrafshan, Y. Mahdavi, Lalhmunsiama, S.M. Lee, Kinetic, isotherms and thermodynamic studies in the removal of 2-chlorophenol from aqueous solution using modified rice straw, Desal. Wat. Treat., 63 (2017) 203–211.

[44] M. Haerifar, S. Azizian, An exponential kinetic model for adsorption at solid/solution interface, Chem. Eng. J., 215–216 (2013) 65–71.

[45] H.C. Thomas, Heterogeneous ion exchange in a flowing system, J. Am. Chem. Soc., 66 (1944) 1664–1666.

[46] S.S. Silva, R.A.S. Ferreira, L. Fu, L.D. Carlos, J.F. Mano, R.L. Reis, J. Rocha, Functional nanostructured chitosan–siloxane hybrids, J. Mater. Chem., 15 (2005) 3952–3961.

[47] S. Loganathan, A.K. Ghoshal, Amine tethered pore-expanded MCM-41: a promising adsorbent for CO₂ capture, Chem. Eng. J., 308 (2017) 827–839.

[48] H. Zhao, T. Zhang, R. Qi, J. Dai, S. Liu, T. Fei, G. Lu, Organic-inorganic hybrid materials based on mesoporous silica derivatives for humidity sensing, Sens. Actuators, B, 248 (2017) 803–811.

[49] M. Thommes, K. Kaneko, A.V. Neimark, J.P. Olivier, F. Rodriguez-Reinoso, J. Rouquerol, K.S.W. Sing, Physisorption of gases, with special reference to the evaluation of surface area and pore size distribution (IUPAC Technical Report), Pure Appl. Chem., 87 (2015) 1051–1069.

[50] D. Pérez-Quintanilla, A. Sánchez, I. Sierra, Preparation of hybrid organic-inorganic mesoporous silicas applied to mercury removal from aqueous media: influence of the synthesis route on adsorption capacity and efficiency, J. Colloid Interface Sci., 472 (2016) 126–134.

[51] C.M. Park, J. Han, K.H. Chu, Y.A.J. Al-Hamadani, N. Her, J. Heo, Y. Yoon, Influence of solution pH, ionic strength, and humic acid on cadmium adsorption onto activated biochar: experiment and modeling, J. Ind. Eng. Chem., 48 (2017) 186–193.

[52] T. Depci, A.R. Kul, Y. Önal, Competitive adsorption of lead and zinc from aqueous solution on activated carbon prepared from Van apple pulp: study in single- and multi-solute systems, Chem. Eng. J., 200–202 (2012) 224–236.

[53] D. Tiwari, H.-U. Kim, S.-M. Lee, Removal behavior of sericite for Cu(II) and Pb(II) from aqueous solutions: batch and column studies, Sep. Purif. Technol., 57 (2007) 11–16.

[54] D. Tiwari, S.P. Mishra, M. Mishra, R.S. Dubey, Biosorptive behaviour of Mango (*Mangifera indica*) and Neem (*Azadirachta indica*) bark for Hg²⁺, Cr³⁺ and Cd²⁺ toxic ions from aqueous solutions: a radiotracer study, Appl. Radiat. Isot., 50 (1999) 631–642.

[55] S.P. Mishra, S.S. Dubey, D. Tiwari, Inorganic particulates in removal of heavy metal toxic ions: IX. Rapid and efficient removal of Hg(II) by hydrous manganese and tin oxides, J. Colloid Interface Sci., 279 (2004) 61–67.

[56] K.F. Hayes, C. Papelis, J.O. Leckie, Modeling ionic strength effects on anion adsorption at hydrous oxide/solution interfaces, J. Colloid Interface Sci., 125 (1988) 717–726.

[57] Thanhmingliana, S.M. Lee, D. Tiwari, S.K. Prasad, Efficient attenuation of 17α-ethynylestradiol (EE2) and tetracycline using novel hybrid materials: batch and column reactor studies, RSC Adv., 5 (2015) 46834–46842.

[58] Y.S. Ho, G. McKay, The kinetics of sorption of divalent metal ions onto sphagnum moss peat, Water Res., 34 (2000) 735–742.